IGF-1 promotes cell surface expression of HCN4 pacemaker channels contributing to tachycardia

Nadine Erlenhardt, Franziska Wohlfarth, S. Erfan Moussavi-Torshizi, Angela Koch, Tobias Strasdeit, Katharina Scherschel, Ehsan Amin, Max Anstötz, Christian Meyer, Nikolaj Klöcker

Journal of Molecular and Cellular Cardiology 210 (2026) 165–174

Contents lists available at ScienceDirect

Journal of Molecular and Cellular Cardiology

journal homepage: www.elsevier.com/locate/yjmcc

IGF-1 promotes cell surface expression of HCN4 pacemaker channels contributing to tachycardia

Nadine Erlenhardt [a,*], Franziska Wohlfarth [a], S. Erfan Moussavi-Torshizi [a], Angela Koch [a], Tobias Strasdeit [a], Katharina Scherschel [a,b], Ehsan Amin [a], Max Anstötz [c], Christian Meyer [b], Nikolaj Klöcker [a,d,*]

[a] Institute of Neural and Sensory Physiology, Medical Faculty and University Hospital, Heinrich Heine University Düsseldorf, Düsseldorf, Germany
[b] Division of Cardiology, Angiology and Intensive Care, EVK Düsseldorf, Cardiac Neuro- and Electrophysiology Research Consortium (cNEP), Düsseldorf, Germany
[c] Institute of Anatomy II, Medical Faculty and University Hospital, Heinrich Heine University Düsseldorf, Düsseldorf, Germany
[d] Cardiovascular Research Institute Düsseldorf (CARID), Medical Faculty and University Hospital Düsseldorf, Heinrich Heine University Düsseldorf, Düsseldorf, Germany

ARTICLE INFO

Keywords:
Insulin-like growth factor-1
Hyperpolarization-activated cyclic nucleotide gated ion channel
Subcellular trafficking
Endocytic recycling compartment
Optical mapping
Extracellular epitope tagging

ABSTRACT

Insulin-like growth factor 1 (IGF-1) controls cardiac growth, metabolism, and contractility. Whereas IGF-1 deficiency is associated with cardiovascular risk, the activation of its signal transduction may be cardioprotective after acute myocardial infarction. Clinical studies evaluate the therapeutic potential of systemic IGF-1 in disease conditions including heart failure, and reported tachycardia as a common side effect. Here, we demonstrate that IGF-1 accelerates cardiac pacemaking in an *ex vivo* mouse sinoatrial node preparation read out by optical voltage mapping. Heterologous reconstitution experiments in *Xenopus laevis* oocytes combining extracellular epitope tagging and electrophysiology reveal an increase in cell surface expression of the main cardiac pacemaker channel isoform HCN4 by IGF-1, which stimulates the Rab11-dependent endosomal recycling of the channel protein. In summary, the study not only adds to the modes of HCN channel regulation by growth factor signaling, but may also extend our understanding of arrhythmogenesis, commonly observed in consequence of IGF-1 dysregulation including cardiac hypertrophy.

1. Introduction

Insulin-like growth factor 1 (IGF-1) is a small peptide hormone of 7.6 kDa sharing *ca.* 50 % homology with pro-insulin [1]. Whereas almost all tissues may produce IGF-1 in an autocrine or paracrine manner, circulating IGF-1 levels are largely synthesized in the liver in response to the hypothalamic growth hormone GH. IGF-1 exerts pleiotropic effects in many organs, including the heart, and affects metabolism, cell proliferation, apoptosis, and autophagy [2,3]. Circulating levels of IGF-1 correlate inversely with the risk of developing cardiovascular disease [4,5], with low IGF-1 levels being associated with a higher risk for coronary artery and ischemic heart disease. Cardiac effects of IGF-1 are mediated by activation of the plasma membrane receptor tyrosine kinase (RTK) IGF-1 receptor (IGF-1R), assumed to signal through two canonical and one non-canonical pathway. The two canonical pathways comprise both PI-3K/AKT and ERK signaling involved in its pro-hypertrophic and pro-survival actions in cardiomyocytes; the non-canonical pathway is postulated to activate phospholipase C (PLC) by a pertussis toxin (PTX) sensitive G protein hydrolyzing membrane phosphoinositides and releasing intracellular calcium ions [2]. Structural organization of IGF-1 signaling domains may add to the complexity of IGF-1R signal transduction [6].

Given the well-established beneficial roles not only in the cardiovascular system [4,7–9], IGF-1 has received attention for therapeutic use. The availability of human recombinant IGF-1 led to new treatments of GH-resistant Laron dwarfism and stimulated clinical trials exploiting its neurotrophic effects [10–12]. However, systemic IGF-1 therapy may be limited by adverse effects as severe as an increased risk of cancer [13], but also by reversible side effects including papilledema, intracranial hypertension, weight gain, and tachycardia [14]. Particularly, an increase in heart rate of up to 15 % for the time of treatment has been reported at high prevalence [15,16]. *In vivo* animal models indicate that

* Corresponding authors at: Institute of Neural and Sensory Physiology, Medical Faculty, University Hospital Düsseldorf, Heinrich Heine University Düsseldorf, Universitätsstr. 1, 40225 Düsseldorf, Germany.
E-mail addresses: nadine.erlenhardt@uni-duesseldorf.de (N. Erlenhardt), nikolaj.kloecker@uni-duesseldorf.de (N. Klöcker).

https://doi.org/10.1016/j.yjmcc.2025.10.015
Received 17 March 2025; Received in revised form 29 September 2025; Accepted 30 October 2025
Available online 1 November 2025

acute administration of IGF-1 decreases the mean arterial pressure by vasodilation and inhibition of constrictor responses, which is accompanied by an increase in heart rate [17–19]. Indeed, the wide molecular range of IGF-1R signaling let us hypothesize that IGF-1 may induce tachycardia by direct modulation of cardiac pacemaking.

Autonomous generation of cardiac action potentials (AP) occurs in specialized pacemaker cells located within the heart [20]. Under physiological conditions, the sinoatrial node (SAN) acts as the primary pacemaker exhibiting the highest frequency of spontaneous AP firing. With HCN4 being the predominant isoform in the human and mouse SAN, hyperpolarization-activated cyclic nucleotide-gated (HCN) channels conduct an inward current, referred to as funny current I_f, which centrally contributes to the slow diastolic depolarization initiating AP generation [21,22]. The strong responsiveness of HCN4 to cAMP, shifting voltage-dependence of its activation to more depolarized values upon C-terminal binding, makes the channel an important subject to chronotropic control by the autonomic nervous system. Increased I_f accelerates heart rate, according to growing experimental evidence most likely by supporting a continuous firing mode in SAN pacemaker cells [23].

Here, we used a mouse *ex vivo* SAN preparation to study the direct effect of IGF-1 on spontaneous pacemaking activity, independent of systemic vascular tone. Optical mapping of the SAN membrane potential revealed an increased AP firing rate after IGF-1 bath application, which was occluded by the HCN channel blockers ZD7288 and ivabradine. Recombinant expression experiments demonstrated an increase in cell surface expression of HCN4 channels by IGF-1-induced phosphorylation of the channel stimulating its endocytic recycling.

2. Materials and methods

2.1. Animals

All animal experiments adhered to the guidelines of the EU Directive 2010/63/EU on the protection of animals used for scientific purposes. The present studies received approval from both the local Animal Care and Use Committee at the University of Düsseldorf (protocol number: O7/11) and the Animal Ethics Committee of the North Rhine-Westphalia Nature, Environment, and Consumer Protection Agency (LANUV). Research involved adult male C57BL/6 J mice, 5 months of age (optical mapping) and 8–10 weeks of age (SAN cell isolation and electrophysiology), obtained from Janvier Labs. Mice were housed under a 12-h light/12-h dark cycle with unrestricted access to water and standard chow diet. All experiments were performed within a consistent time window each day (±2 h) to control for circadian variations in cardiac electrophysiology.

2.2. Tissue staining

Euthanasia of mice was performed through cervical dislocation. Cardiac tissue was promptly excised and submerged in an ice-cold oxygenated (95 % O_2, 5 % CO_2) bicarbonate-buffered extracellular solution (ECS, in mM: 123 NaCl, 1.8 $CaCl_2$, 5.4 KCl, 1.2 $MgCl_2$, 1.4 NaH_2PO_4, 24 $NaHCO_3$, and 10 glucose). After tissue excision, retrograde perfusion of the aorta with ECS was initiated using a peristaltic pump to maintain a steady flow rate of 1.5 ml/min. This initial perfusion, lasting a minimum of 4 min, was crucial to restore rhythmic contractions in the isolated cardiac tissues. Subsequently, 3.6 μM Di-4-ANBDQPQ (6152, Cyto Cybernetics) in ECS was perfused for 4 min to stain the tissue. After successful dye-loading, continuous perfusion with 10 μM (−)-blebbistatin (S7099, Selleckchem) in ECS was maintained until cardiac contractions ceased.

2.3. Atrial isolation and SAN exposing preparation

To optically map membrane voltage from sinoatrial node (SAN) cells, the atria were isolated from the heart and the SAN was exposed. To this end, the ventricles were dissected from the anterior side of the atrial preparation, with the left ventricle removed. A precise incision was made along the tricuspid valve (TV) following the TV-superior vena cava axis to open the right atrium (RA). An incision through the medial limb of the crista terminalis allowed access to the right atrial appendage (RAA). Finally, a cut was made along the anterior atrial free wall, extending from the midpoint of the RAA to its lower right corner, enabling the RA to be flattened and fully exposing the SAN. The specimen was then transferred to a custom circulation chamber filled with oxygenated (95 % O_2, 5 % CO_2) ECS, supplemented with 10 μM (−)-blebbistatin. The solution temperature was maintained at 35 °C by passing it through a glass spiral before entering the chamber, while the flow rate was regulated at 6 ml/min. To minimize movement and ensure optimal conditions for data collection, the tissue was securely flattened using 0.1 mm pins.

2.4. Optical mapping

To optically record action potentials, a THT Macroscope (SciMedia/Brainvision) was employed [24]. Briefly, a LED light source (LEX3-G; 525 nm; SciMedia/Brainvision) passed light through an excitation filter (BP531 nm/40) before being redirected by a dichroic mirror (580-FDI) toward the perfusion chamber, where it was focused onto the flattened SAN. Emitted fluorescent signals were filtered by a long-pass filter (LP730 nm) and captured by a MiCAM05-N256 imaging system (SciMedia/Brainvision) equipped with a CMOS image sensor (mapping field area: 10 × 10 mm, 256 × 256 pixels, frame rates: 1 kHz; SciMedia/Brainvision). Recordings were operated by the proprietary BV Workbench (Brainvision), and customized MATLAB scripts were used for analysis. Data acquisition started once the frequency of SAN action potentials had stabilized. 20 min later, a second dataset was collected under distinct conditions: (1) no drug treatment, (2) in the presence of 500 nM insulin-like growth factor 1 (IGF-1), (3) in the presence of 20 μM ZD7288, (4) in the presence of both 500 nM IGF-1 and 20 μM ZD7288, (5) in the presence of both 500 nM IGF-1 and 2 μM ivabradine, and (6) in the presence of both 500 nM IGF-1 and 1 μM picropodophyllin. The comparison of the basic cycle length (BCL) was conducted between the initial and second datasets, as well as between the groups with no treatment, IGF-1, ZD7288 + IGF-1 or ivabradine + IGF-1.

2.5. Isolation and electrophysiological recordings from mouse SAN cells

SAN cells were isolated following the protocol by Fenske et al. [25]. In brief, SANs were excised from hearts of 8–10 week old male C56BL/6 J mice and enzymatically digested with a mixture of elastase (18.87 U), protease (1.79 U) and collagenase B (0.54 U) in Tyrode low (in mM: 140 NaCl, 5.4 KCl, 0.5 $MgCl_2$, 0.2 $CaCl_2$, 1.2 KH_2PO_4, 50 taurine, 5 HEPES, 5.5 glucose, pH 7.4) for 30 min at 36 °C and 600 rpm. After termination of enzymatic digestion, tissue was incubated at 4 °C for 2.5 h in Kraftbrühe (in mM: 80 L-glutamic acid, 25 KCl, 3 $MgCl_2$, 10 KH_2PO_4, 20 taurine, 10 HEPES, 0.5 EGTA, 10 glucose, pH 7.4) before titruation and seeding cells onto poly-L-lysin-coated coverslips. After 15 min, Ca^{2+} concentration was gradually increased to physiological Ca^{2+} levels and cells were subjected to electrophysiological recordings.

Whole-cell voltage-clamp recordings from isolated SAN cells were performed using glass electrodes filled with an internal solution containing (in mM): 130 KCl, 10 NaCl, 0.5 $MgCl_2$, 5 EGTA, 5 HEPES, 3 Mg-ATP, 0.5 Na-GTP, and 0.1 cAMP (pH adjusted to 7.2). Coverslips with dissociated cells were continuously superfused with oxygenated artificial cerebrospinal fluid (ACSF) containing (in mM): 140 NaCl, 5.4 KCl, 1 $MgCl_2$, 1 $CaCl_2$, 0.3 $CdCl_2$, 2 $BaCl_2$, 5 HEPES, and 5 glucose, bubbled with 95 % O_2 and 5 % CO_2 at 30 °C.

For IGF-1 experiments, 50 nM IGF-1 was added to the ACSF, and cells were incubated for at least 10 min prior to recordings.

SAN cells were held at a membrane potential of −40 mV. Currents

were leak-subtracted and normalized to cell capacitance. To record I_f current, a voltage step to −130 mV was applied for 4.5 s. I_f amplitudes were measured at the end of the activating voltage step. To obtain the voltage-dependent activation curve, a series of voltage steps was applied, ranging from −40 mV to −140 mV in 20 mV increments, each lasting 4.5 s. Tail currents were elicited by a final step to −140 mV. Tail current amplitudes were leak-corrected, normalized, and fitted using a Boltzmann equation: $(I - I_{min})/(I_{max} - I_{min}) = 1/[1 + exp.((V_{0.5} - V_m)/k)]$, where V_m is the membrane potential, $V_{0.5}$ is the half-activation voltage, and k is the slope factor.

For whole-cell current-clamp recordings isolated SAN cells were continuously superfused with Tyrode III solution containing (in mM): 140 NaCl, 5.4 KCl, 1 $MgCl_2$, 1.8 $CaCl_2$, 5 Hepes, 5.5 glucose, pH 7.4, bubbled with 95 % O_2 and 5 % CO_2 at 30 °C.

2.6. Molecular biology

The cDNA coding for human HCN4 (hHCN4) channel (AJ132429.1) was subcloned into pGEM-He for expression in *Xenopus laevis* oocytes using *Eco*RI and *Xba*I. Point mutants were generated by polymerase chain reaction (PCR)-directed mutagenesis with specific mismatch primers (biomers.net) or by using QuikChange II Site-Directed Mutagenesis Kit (Agilent Technologies) with specific primers and confirmed by sequencing. The extracellular haemagglutinin (HA) epitope tagging was performed as described previously [26]. cRNA was synthesized from 1 µg of linearized plasmid DNA using an *in vitro* transcription kit (mMESSAGE mMACHINE® T7 Transcription Kit, Thermo Fisher Scientific).

2.7. Heterologous expression of HCN4 in Xenopus laevis oocytes

Xenopus laevis oocytes of stages V-VI were purchased from EcoCyte Bioscience (Castrop-Rauxel, Germany) and maintained in Barth's solution (in mM: 88 NaCl, 1 KCl, 2.4 $NaHCO_3$, 0.82 $MgSO_4$, 0.41 $CaCl_2$, 0.33 $Ca(NO_3)_2$, 20 HEPES, pH adjusted to 7.5 with NaOH) charged with antibiotic and antimycotic solution (containing penicillin, streptomycin and amphotericin B, Sigma-Aldrich) at 18 °C. Oocytes were injected with 6–20 ng HCN4 cRNA using a Micro4 nanoliter injector (World Precision Instruments, Sarasota, FL, USA).

2.8. Electrophysiological recordings from Xenopus laevis oocytes

Two-electrode voltage clamp (TEVC) recordings of oocyte current responses were performed 3–4 days after cRNA injection with a Turbo Tec-03× amplifier (npi electronic, Germany) controlled by Pulse software (HEKA, Germany). Electrodes were filled with 3 M KCl and had resistances of 0.5–1.5 MΩ. Oocytes were superfused with HCN4 Ringer's solution (in mM: 17.5 NaCl, 115 KCl, 1.8 $CaCl_2$ and 10 HEPES, pH 7.3) at −20 mV holding potential and the channels were activated with a − 150 mV pulse for 7 s before and after incubation with 50 nM IGF-1 or 20 µM SC79 for 30 min. The voltage-dependent activation curve was determined by a series of activating voltage steps (5 s each) ranging from −20 mV to −150 mV in 10 mV increments. A following step to −150 mV for 2 s elicited the tail current.

2.9. Quantification of HCN4 surface expression in Xenopus laevis oocytes

All steps were performed at 4 °C with gentle shaking and in the absence of detergents. Briefly, oocytes were pre-treated with 1 % bovine serum albumin (BSA) in Barth's solution for 30 min and incubated with primary anti-HA antibody (1:100, Santa Cruz) followed by incubation with horse-radish peroxidase conjugated goat anti-mouse secondary antibody (1:5.000, Abcam). Immunoreactivity was detected by enzymatic turnover of SuperSignal ELISA Femto Maximum Sensitivity Substrate (Thermo Scientific) and quantified in a Glomax 20/20 n luminometry system (Promega).

2.10. SDS-PAGE and Western blotting

Whole cell lysates from *Xenopus laevis* oocytes were separated on 10 % SDS-PAGE gels and transferred to PVDF membranes using the Mini-PROTEAN system from Bio-Rad. Western analysis was performed using the following primary antibodies: rabbit anti-HCN4 (Alomone) and rabbit anti-β-Actin (Abcam). After incubation with goat anti-rabbit secondary antibodies conjugated to horseradish peroxidase (Santa Cruz) blots were developed with ECL prime (GE Healthcare).

2.11. Immunohisto- and cytochemistry

Staining of atrial whole-mount preparations was performed as previously described [27]. Hearts were formalin-fixed for 48 h at room temperature. Atria were dissected and atrial fat tissue re-moved before bleaching in Dent's bleach (MeOH:DMSO:H_2O_2 4:1:1) for 2 h at room temperature. Samples were rehydrated in a descending methanol series, and permeabilized for 2 h in 1 % Triton X-100 in PBS. Blocking was performed for 2 h in blocking buffer (5 % bovine serum albumin/0.1 % Triton X-100/PBS), before primary antibody incubation for 72 h at room temperature in blocking buffer (rabbit-anti-HCN4, APC-052, Alomone Labs). Specimen were washed 6 × 30 min in 0.1 % Triton X-100/PBS, followed by secondary antibody incubation in 0.1 % Triton X-100/PBS for 48 h at room temperature (donkey-anti-rabbit IgG Alexa Fluor 568, A11057, life technologies). Samples were washed for 2 × 30 min in 0.1 % Triton X-100/PBS. To decrease autofluorescence, Sudan black (0.25 % in 70 % ethanol) staining was performed for 2 h at RT. After rehydration in a descending ethanol series, samples were kept in PBS for imaging with a Leica stereomicroscope M205 (Leica Microsystems GmbH, Wetzlar, Germany).

Immunocytochemistry of isolated SAN cells was performed as follows: cells were fixed in 4 % paraformaldehyde for 20 min and permeabilized in 1 % Triton X-100/PBS for 10 min, before blocking in 10 % normal goat serum/PBS for 1 h. Cells were incubated in primary antibody (rabbit-anti-HCN4, APC-052, Alomone Labs) for 1 h, followed by brief washing in PBS and a 1 h incubation in secondary antibody (goat-anti-rabbit IgG Alexa Fluor 647, A21244, Life Technologies) and rhodamine phalloidine (R415, Life Technologies). Cells were washed 3 × 5 min and mounted in ProLong diamond (Life Technologies).

Confocal imaging was performed with a LSM710 (Carl Zeiss Microscopy, Wetzlar, Germany) using a Plan-Apochromat 63×/1,4 Oil DIC M27 objective.

2.12. Statistics

Data are given as mean ± SEM unless otherwise stated. n refers to the number of oocytes (from a minimum of 2 different batches) or the number of SAN preparations, respectively. Statistical analysis was performed using GraphPad Prism 10 (GraphPad Softwares, San Diego, USA). Normal distribution of data was confirmed using a Shapiro-Wilk or Kolmogorov-Smirnov test. Data were then analyzed using a paired or unpaired Student's *t*-test or a parametric ANOVA followed by a multiple comparisons test as indicated in the figure legends. Level of statistical significance was defined as * = $p < 0.01$ for data obtained from Xenopus oocytes and * = $p < 0.05$ for data obtained from native SAN preparations.

3. Results

In order to test the hypothesis that IGF-1 may increase heart rate by direct modulation of sinuatrial pacemaker activity, we employed an *ex vivo* SAN whole-mount preparation, from which spontaneously generated action potentials (AP) were recorded by optical voltage mapping (Fig. 1). Under control conditions, the basic cycle length (BCL) was 322.5 ± 35.49 ms ($n = 6$). Bath application of 500 nM IGF-1 significantly decreased BCL to 199.5 ± 22.07 ms within 20 min time

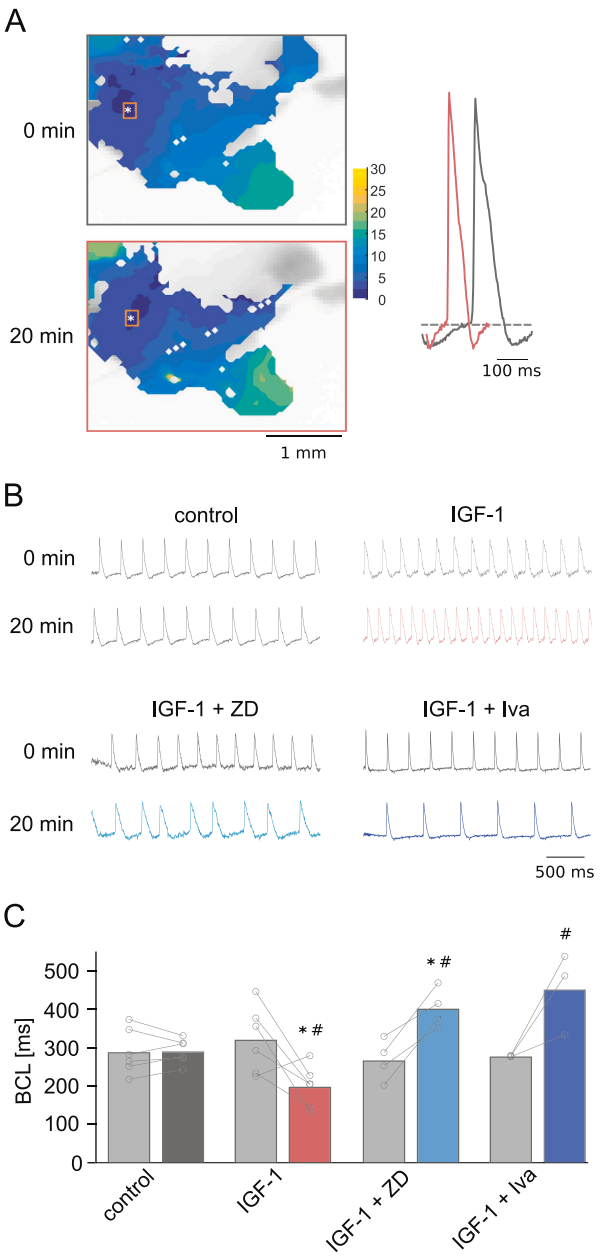

Fig. 1. IGF-1 increases the frequency of spontaneous action potentials in an *ex vivo* SAN preparation. A Left: representative activation maps of an *ex vivo* SAN preparation before (grey) and 20 min after application (red) of 500 nM IGF-1 by optical mapping of membrane voltage. White asterisks indicate SAN, orange boxes mark the regions used for analyzing action potentials. Right: Overlay of spatially (orange boxes) and temporally (3 s) averaged representative optical action potentials (OAPs) before (grey) and 20 min after (red) incubation with IGF-1. Dashed line marks OAP threshold. B Representative recordings of spontaneously generated action potentials from an *ex vivo* SAN preparation by optical mapping of membrane voltage, before (grey) and 20 min after application of either control solution (dark grey), 500 nM IGF-1 (red), 500 nM IGF-1 + 20 μM ZD7288 (light blue) or 500 nM IGF-1 + ivabradine (dark blue). C Quantification of the basic cycle length (BCL) for the respective datasets, given as mean ± SEM: control solution (before: 292.0 ± 13.20 ms, 20 min: 322.5 ± 35.49 ms, $p = 0.8850$, $n = 6$), IGF-1 (before: 322.5 ± 35.49 ms, 20 min: 199.5 ± 22.07 ms, $p = 0.0355$, $n = 6$), IGF-1 + ZD7288 (before: 268.5 ± 26.91 ms, 20 min: 403.8 ± 25.56 ms, $p = 0.0116$, $n = 4$, ZD), IGF-1 + ivabradine (before: 278.0 ± 1.155, 20 min: 453.7 ± 61.62, $p = 0.1010$, $n = 3$, Iva). BCL was compared between the respective datasets (paired Student's *t*-test, significant changes marked with an asterisk), as well as between the second datasets of the control group and the groups with IGF-1 ($p = 0.0488$), IGF-1 + ZD7288 ($p = 0.0393$) or IGF-1 + ivabradine ($p = 0.0033$) respectively (ordinary one-way ANOVA followed by a Sidák's multiple comparisons test, significant changes marked with a rhomb). (For interpretation of the references to colour in this figure legend, the reader is referred to the web version of this article.)

translating into an increase in AP frequency by *ca.* 62 % (n = 6, $p = 0.0355$). Reducing the cardiac pacemaker current I_f by the HCN channel blockers ZD7288 (20 μM) or ivabradine (2 μM) occluded any effect of simultaneous IGF-1 application, yielding a BCL of 403.8 ± 25.56 ms ($n = 4$, $p = 0.0393$) and of 453.7 ± 61.62 ($n = 3$, $p = 0.0033$), respectively. Likewise, the IGF-1 receptor blocker picropodophyllin (PPP, 1 μM; [28]) prevented the effects of IGF-1 on BCL (Fig. S1). All pharmacologically induced changes in BCL differed also from control recordings after 20 min confirming stable experimental conditions. Thus, IGF-1 increased the frequency of spontaneously generated AP in an *ex vivo* SAN preparation, most likely by direct modulation of I_f.

We therefore sought to directly record I_f from SAN cells in the absence or presence of IGF-1. As shown in Fig. 2, 50 nM IGF-1 increased I_f current amplitudes (@ -130 mV, 4.5 s, 100 μM cAMP) from 9.66 ± 2.17 pA/pF ($n = 19$) to 15.27 ± 3.20 pA/pF ($n = 21$, $p = 0.020$) without affecting its voltage-dependent activation. To further elucidate

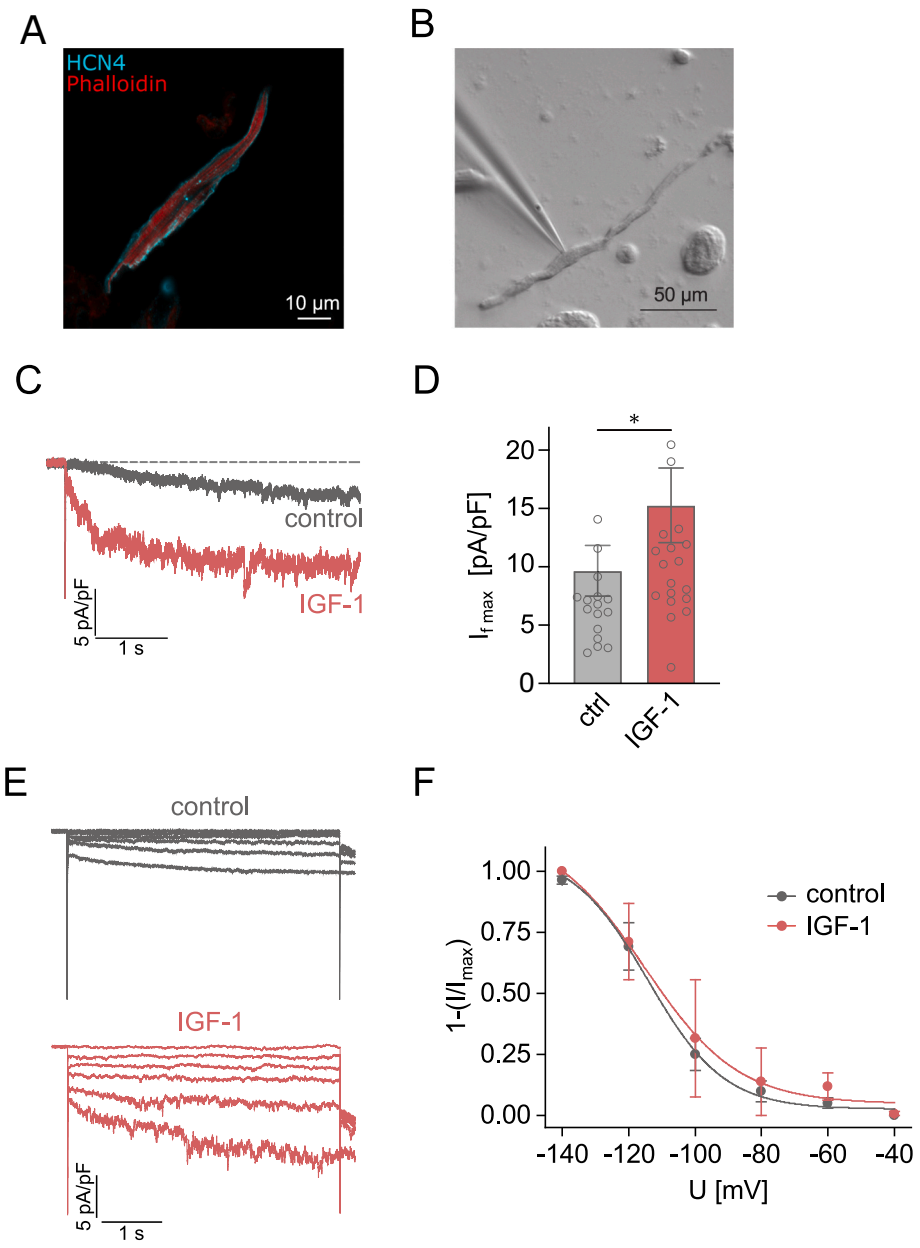

Fig. 2. IGF-1 increases I_f current amplitudes in isolated SAN pacemaker cells. A Representative confocal image of an isolated elongated-type SAN cell stained for HCN4 immunoreactivity (cyan) and phalloidin (red) showing HCN4 expression in its plasma membrane. B Representative micrograph of an isolated SAN pacemaker cell (elongated-type) for patch clamp experiments. C Representative whole-cell I_f currents from isolated SAN cells in the absence (grey) and presence (red) of 50 nM IGF-1 elicited by a voltage step from $V_h = -40$ mV to −130 mV for 4.5 s in the presence of 100 µM cAMP (filtered at 300 Hz). D Quantification of maximal I_f amplitudes at −130 mV (4.5 s) in the absence (grey) and presence (red) of 50 nM IGF-1. IGF-1 treatment significantly increased I_f current amplitudes from 9.66 ± 2.17 pA/pF ($n = 18$) to 15.27 ± 3.20 pA/pF ($n = 21$, $p = 0.0204$, Mann Whitney test). Outliers exceeding 25 pA/pF were removed from the graph to improve visual clarity (5 total (control: 2 and IGF-1: 3)). E Representative whole-cell I_f currents recorded from isolated SAN cells in the absence (grey) or presence (red) of 50 nM IGF-1 (filtered at 300 Hz, see Materials and Methods). F Voltage-dependent activation of I_f, fitted with a sigmoidal Boltzmann function, showing no significant change between recordings from control (grey: $V_{0.5} = -114.16 \pm 1.94$ mV, $k = 11.45 \pm 1.65$ mV, $n = 4$) and IGF-1 treated pacemaker cells (red: $V_{0.5} = -115.2 \pm 5.63$ mV, $k = 14.11 \pm 4.16$ mV, $n = 4$). (For interpretation of the references to colour in this figure legend, the reader is referred to the web version of this article.)

underlying molecular mechanisms, we heterologously expressed the main cardiac pacemaker channel isoform HCN4 in *Xenopus laevis* oocytes and recorded current amplitudes at maximum voltage activation by TEVC ($V_h = -150$ mV, 7 s). As depicted in Fig. 3, bath application of 50 nM IGF-1 increased HCN4 current amplitudes by a factor of 2.42 ± 0.24 after 30 min incubation ($n = 16$, $p < 0.0001$). A closer look at the time course of the increase in HCN4 current induced by IGF-1 revealed a time scale of minutes when recorded at room temperature (Fig. 3C/D). Using an extracellular epitope tagging approach, we observed a strong increase in cell surface expression of extracellularly HA-tagged HCN4 by a factor of 3.1 ± 0.36 after 30 min ($n = 22$–23, $p < 0.0001$), whereas total protein expression remained unaffected ($n = 3$), as did voltage-dependence ($n = 16$ (WT), $n = 8$ (WT + IGF-1)) and kinetics ($n = 15$ (WT), $n = 8$ (WT + IGF-1)) of activation of HCN4 (Fig. 3E/F; Fig. S3A).

Canonical IGF-1 signaling involves activation of the PI3K/AKT pathway [2]. Former phosphoproteomic analysis had identified four AKT-sensitive phosphorylation sites contained in the cytoplasmic N-terminus of HCN4 [29]. We hence designed two HCN4 mutants, a phospho-mimicking mutant by exchanging the four serine residues (S14, S99, S102, S139) for aspartate (SD) and a phospho-ablative mutant by

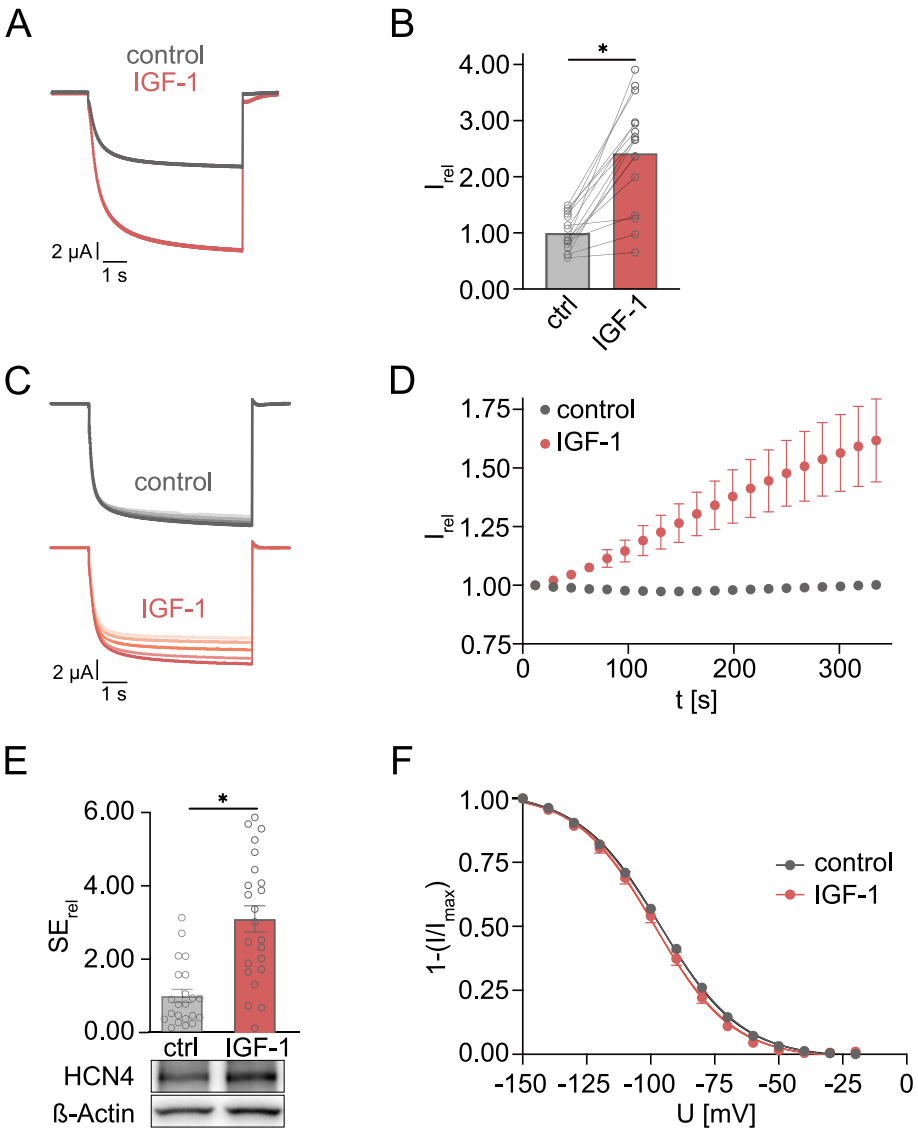

Fig. 3. IGF-1 increases HCN4 current amplitudes in *Xenopus laevis* oocytes by promoting channel surface expression. A Representative current responses from HCN4 expressing *Xenopus laevis* oocytes before (grey) and after a 30 min incubation with 50 nM IGF-1 (red) recorded by TEVC. Oocytes were clamped at a holding potential of −20 mV and channels were activated by a voltage-step to −150 mV for 7 s. B Quantification of normalized HCN4 current amplitudes before (grey) and after IGF-1 incubation (red). IGF-1 significantly increased HCN4 currents by a factor of 2.42 ± 0.24 ($n = 16$, $p < 0.0001$). C Representative HCN4 current traces of oocytes without (control, grey) and during (IGF-1, red) a *ca.* 5 min incubation with 50 nM IGF-1. During this time, maximal channel activation by a voltage-step to −150 mV was repeated 20 times. D Relative current amplitudes during repeated maximal activation of HCN4 in the presence or absence of 50 nM IGF-1. Note the IGF-1 mediated increase in current amplitude on a time scale of minutes. E Quantification of HCN4 surface expression using an extracellular epitope tagging approach. Incubation with IGF-1 increased HCN4 cell surface expression (3.099 ± 0.36, $n = 23$) compared to control oocytes (1.00 ± 0.18, $n = 22$; unpaired Student's *t*-test: $p < 0.0001$). A representative Western blot shows no change in total HCN4 expression after IGF-1 treatment. ß-actin served as loading control. F Voltage-dependent activation of HCN4 channels, fitted with a sigmoidal Boltzmann function, with no significant changes between control (grey, $V_{0.5} = -96.46 \pm 0.45$ mV, slope: −16.13 ± 0.44 mV, $n = 16$) and after incubation with IGF-1 (red, $V_{0.5} = -98.37 \pm 0.68$ mV, slope: −14.98 ± 0.64 mV, $n = 8$). (For interpretation of the references to colour in this figure legend, the reader is referred to the web version of this article.)

exchanging them for alanine (SA). Fig. 4 shows that the increase in HCN4 current amplitudes induced by IGF-1 was sensitive to the introduced mutations, with SD anticipating, and SA preventing most of the IGF-1 mediated potentiation, indicating partial phosphorylation of these residues in wild-type channels already under control conditions. Whereas wild-type HCN4 current amplitudes were strongly increased from 3.16 ± 0.57 µA to 8.18 ± 0.93 µA by incubation with IGF-1 for 30 min ($n = 10$, $p < 0.0001$), SD current amplitudes started at 7.18 ± 1.66 µA and could only be amplified to 8.07 ± 1.77 µA by IGF-1 ($n = 7$, $p = 0.01$). SA current amplitudes were 2.06 ± 0.49 µA and increased to only 3.08 ± 0.66 µA after IGF-1 incubation ($n = 5$, $p = 0.0051$). Small molecule activation of cytosolic AKT by SC79 was able to potentiate wild-type HCN4 current amplitudes after incubation for 30 min, indeed to far lesser extent than IGF-1 did (Fig. S4). SA current amplitudes were not significantly amplified by SC79.

We finally sought to gain more insight into the mechanism by which IGF-1 may increase cell surface expression of HCN4. We had reported before that HCN4 traffics through the endocytic recycling compartment (ERC) in a Rab11-dependent manner [26]. Sequence information contained in the HCN4 C-terminus is both necessary and sufficient to direct the channel into the ERC, which may serve regulated and rapid adaptation of its cell surface expression. In the present study, we observed strong sensitivity of HCN4 current and its increase induced by IGF-1 to dominant-negative Rab11 (Rab11 S25N), whereas upon co-expression

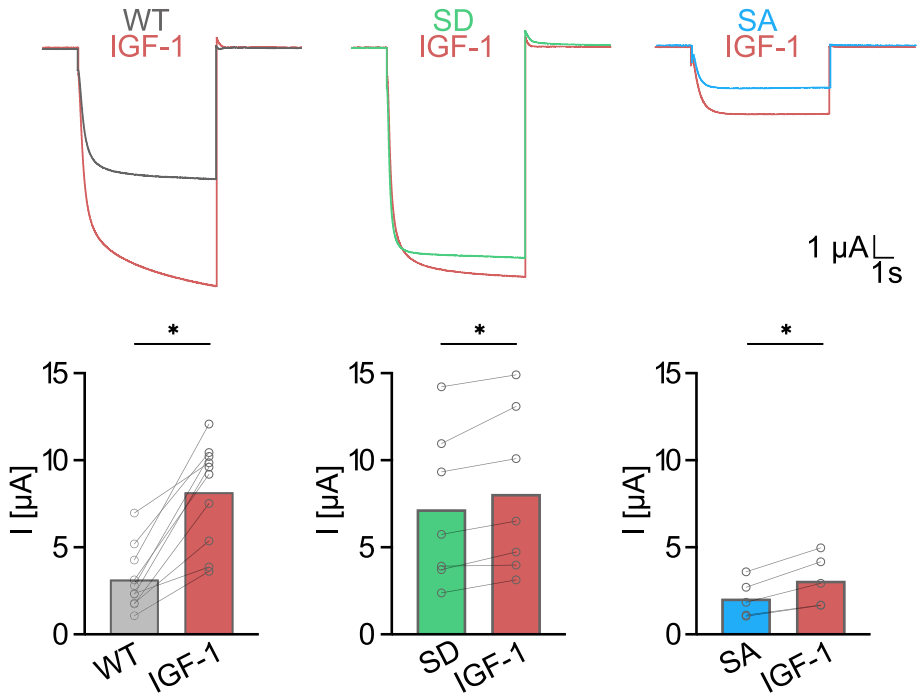

Fig. 4. The increase in HCN4 current amplitudes is due to IGF-1-dependent channel phosphorylation. Representative current traces from HCN4 WT (grey), SD (green) or SA (blue) mutants expressed in *Xenopus laevis* oocytes before and after (red) incubation with 50 nM IGF-1. Bar graphs show quantification of the respective current amplitudes. HCN4 WT current amplitudes were increased from 3.16 ± 0.57 µA to 8.18 ± 0.93 µA by IGF-1 ($n = 10$, $p < 0.0001$), SD current amplitudes started at 7.18 ± 1.66 µA and were further amplified to 8.07 ± 1.77 µA by IGF-1 ($n = 7$, $p = 0.01$). SA current amplitudes started at 2.06 ± 0.49 µA and increased to 3.08 ± 0.66 µA after IGF-1 incubation ($n = 5$, $p = 0.0051$). (For interpretation of the references to colour in this figure legend, the reader is referred to the web version of this article.)

of dominant-negative dynamin (Dyn K44A) only the IGF-1 induced increase in HCN4 current amplitude was significantly attenuated (Fig. 5A). Thus, Rab11 S25N decreased HCN4 current amplitudes from 9.15 ± 0.72 µA to 2.99 ± 0.4 µA before and from 16.38 ± 0.333 µA to 5.00 ± 0.5 µA after 30 min incubation with IGF-1 ($n = 12$, $p < 0.0001$ and $n = 12$, $p < 0.0001$, respectively). In contrast, Dyn K44A decreased HCN4 current amplitudes potentiated by IGF-1 from 9.95 ± 0.71 µA to 3.93 ± 0.24 µA ($n = 10$–11, $p < 0.0001$) much stronger than naïve HCN4 current amplitudes, from 3.59 ± 0.4 µA when co-expressed with wild-type dynamin to 2.23 ± 0.19 µA when co-expressed with Dyn K44A ($n = 10$ and $n = 11$, respectively, $p = 0.053$). These findings were mimicked by the two HCN4 mutants, with SD being sensitive to both Rab11 S25N and Dyn K44A, whereas SA was sensitive only to Rab11 S25N but not to Dyn K44A (Fig. 5B). Co-expression of Rab11 S25N reduced SD current amplitudes from 6.48 ± 0.48 µA to 2.84 ± 0.16 µA ($n = 12$ and $n = 14$, respectively, $p < 0.0001$) and SA amplitudes from 3.92 ± 0.30 µA to 1.37 ± 0.09 µA ($n = 13$ and $n = 11$, respectively, $p < 0.0001$). In contrast, Dyn K44A only reduced SD from 9.14 ± 0.69 µA to 3.62 ± 0.22 µA ($n = 21$ and $n = 15$, respectively, $p < 0.0001$), leaving SA unaffected (3.95 ± 0.25 µA and 4.43 ± 0.38 µA, respectively, $n = 29$ and $n = 19$, $p = 0.878$). Altogether, these data suggest that IGF-1 increased cell surface expression of HCN4 by promoting its ERC recycling.

4. Discussion

The present study demonstrates that IGF-1 promotes cell surface expression of the pacemaker channel HCN4, which may contribute to accelerating heart rate. Besides adding to the highly diverse modes of HCN channel regulation, our study provides novel mechanistic insight, which may explain the side effect of tachycardia frequently observed in patients receiving systemic IGF-1 treatment.

In an *ex vivo* SAN wholemount preparation, bath application of IGF-1 increased spontaneous AP firing, which was precluded by the HCN channel blockers ZD7288 and ivabradine. As samples were denervated, these data strongly indicate direct action of IGF-1 on I_f. However, the presented results do not exclude effects of IGF-1 on other ionic currents that may either feed into the slow diastolic depolarization or AP repolarization, eventually governing heart rate. Also not excluded may be effects of IGF-1 on the dynamic interaction of cells within the SAN complex [30]. Indeed, recordings from isolated SAN pacemaker cells under saturating cyclic nucleotide concentration exhibited an increase in I_f current density after IGF-1 incubation. As voltage-dependent activation of I_f remained unaffected, the increase in its current density may be deduced to either an increase in channel numbers on the cell surface or in single channel conductance. In order to gain more mechanistic insight, we expressed the main pacemaker channel isoform HCN4 in the heterologous expression system of *Xenopus laevis* oocytes, and recorded currents in TEVC mode warranting saturated levels of the two allosteric HCN gating effectors, the cyclic nucleotide cAMP and plasma membrane phosphoinositides [31–33]. On a time scale of only few minutes, IGF-1 was able to increase HCN4 current several fold. By exploiting an extracellular epitope tagging approach, a concomitant increase in cell surface expression of HCN4 was detected, whereas its voltage-dependent gating remained again unaffected. The short time scale of events at room temperature renders new biosynthesis of channel protein unlikely. Thus, we conclude that IGF-1 enhances HCN4 current by regulating the subcellular trafficking of the conducting channels.

In good agreement with a former phosphoproteomic analysis of HL-1 cells [29], which had identified four N-terminal serine residues in HCN4 being phosphorylated in an AKT-dependent manner, the IGF-1 mediated increase in HCN4 current was largely anticipated by a phospho-mimicking HCN4 mutant (SD), whereas it was largely abolished by a phospho-ablative mutant (SA). Supporting the hypothesis that AKT-dependent channel phosphorylation promotes HCN4 cell surface expression, the small molecule AKT activator SC79 also enhanced HCN4 current, albeit to much lesser extent than IGF-1. This may be due to the

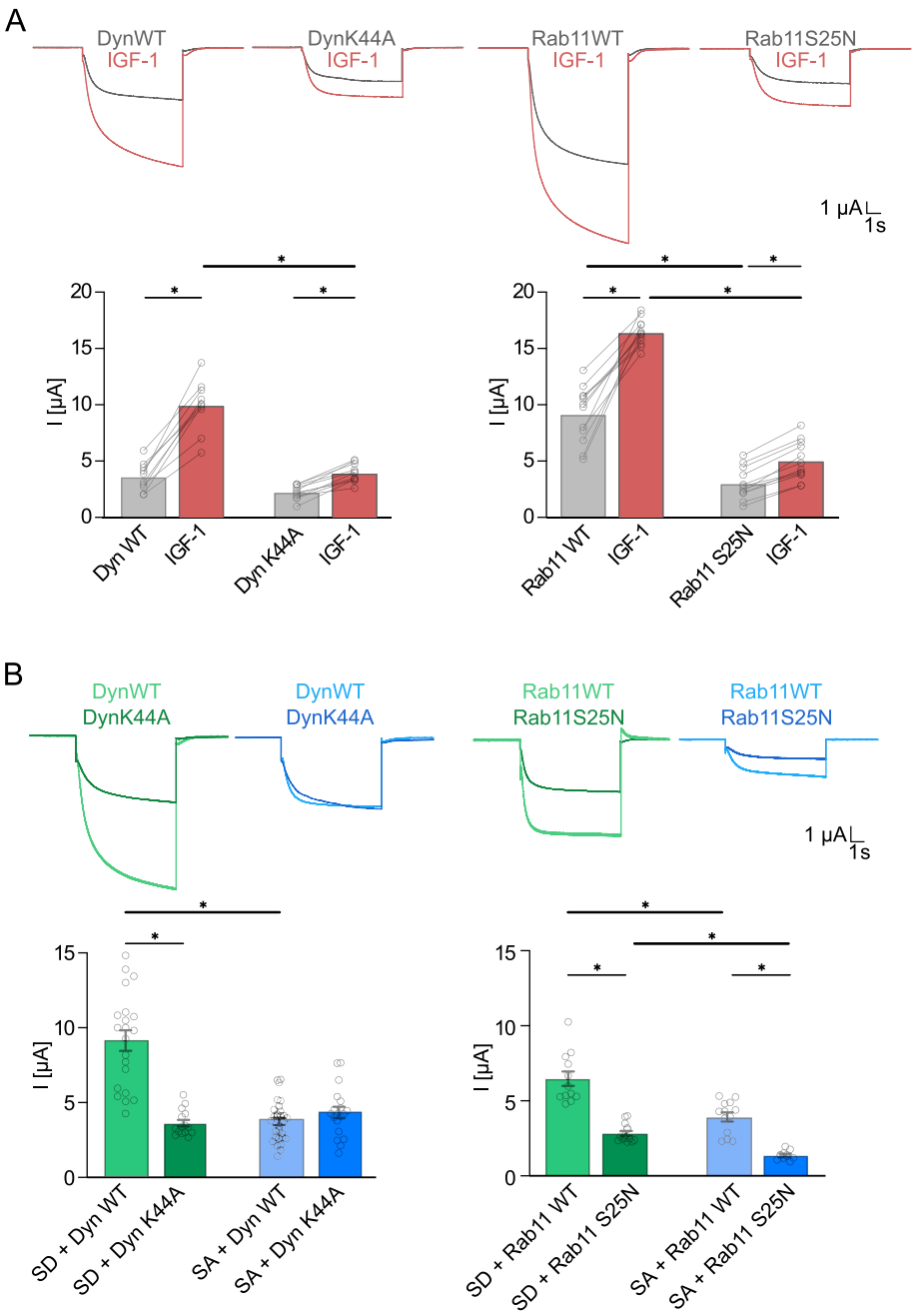

Fig. 5. IGF-1 increases HCN4 channel surface expression by promoting its ERC recycling. A Representative current traces and quantification of current amplitudes recorded from *Xenopus laevis* oocytes expressing HCN4 WT with either Dyn WT or Dyn K44A, or together with Rab11 WT or Rab11 S25N, before (grey) and after (red) a 30 min incubation with IGF-1, respectively. Dyn K44A decreased HCN4 current amplitudes potentiated by IGF-1 from 9.95 ± 0.71 µA (Dyn WT, n = 10) to 3.93 ± 0.24 µA ($n = 11$, $p < 0.0001$). HCN4 current amplitudes before IGF-1 treatment were only reduced from 3.59 ± 0.4 µA (Dyn WT, $n = 10$) to 2.23 ± 0.19 µA when co-expressed with Dyn K44A ($n = 11$, $p = 0.053$). Rab11 S25N decreased HCN4 current amplitudes compared to Rab11 WT from 9.15 ± 0.72 µA to 2.99 ± 0.4 µA before ($n = 12$, $p < 0.0001$) and from 16.38 ± 0.33 µA to 5.00 ± 0.5 µA after IGF-1 treatment ($n = 12$, $p < 0.0001$). Current amplitudes were compared before and after IGF-1 treatment using a paired Student's *t*-test and between groups applying an ordinary one-way ANOVA followed by a Sidák's multiple comparisons test. B Representative current traces and bar graphs showing quantification of current amplitudes recorded from *Xenopus laevis* oocytes expressing HCN4 SD (green) or HCN4 SA (blue) with either Dyn WT or K44A or Rab11 WT or S25N, respectively. Dyn K44A only reduced SD from 9.14 ± 0.69 µA to 3.62 ± 0.22 µA (Dyn WT: $n = 21$ and Dyn K44A: $n = 15$, $p < 0.0001$), leaving SA unaffected (Dyn WT: 3.95 ± 0.25 µA, $n = 29$ and Dyn K44A: 4.43 ± 0.38 µA, $n = 19$, $p = 0.878$).In contrast, co-expression of Rab11 S25N reduced SD current amplitudes from 6.48 ± 0.48 µA (Rab11 WT, $n = 12$) to 2.84 ± 0.16 µA ($n = 14$, $p < 0.0001$) and SA current amplitudes from 3.92 ± 0.30 µA (Rab11 WT, $n = 13$) to 1.37 ± 0.09 µA ($n = 11$, $p < 0.0001$). Data were analyzed using an ordinary one-way ANOVA followed by a Sidák's multiple comparisons test. (For interpretation of the references to colour in this figure legend, the reader is referred to the web version of this article.)

fact that an increase in cell surface expression occurs most notably, when surface HCN4 is phosphorylated in an AKT-dependent manner. SC79, however, activates AKT only in the cytosol and even prevents translocation to the plasma membrane by binding to its PH domain [34]. Whether AKT directly phosphorylates the HCN4 N-terminus or whether AKT effector kinases, *e.g.* GSK3, are involved remains somewhat elusive [35]. Only the serine residue S14 fully matches the canonical consensus sequence of AKT phosphorylation (RXRXXS/T), residues S99 and S102 fit its basic pattern after all, whereas S139 conforms least to it. Addressing this question becomes rather complex, as the

phosphorylation status of AKT itself regulates its substrate selectivity [36] and as residues S14 and S99 have been identified to be also phosphorylated by PKA *in vitro* [37].

We have previously reported that HCN4 bears sequence information in its C-terminal domain, which is both necessary and sufficient to enter the endocytic recycling pathway [26]. As known for many membrane receptors, the ERC may serve as an intracellular storage compartment to maintain homeostatic surface expression, but also to supply preformed channels for its rapid adaptation in response to extracellular stimuli [38]. Mathematical models distinguishing between surface and intracellular pools of a given membrane protein under steady-state conditions predict a proportional relation of the size of the surface pool to the recycling rate of the protein, whereas its rates of endocytosis and degradation relate inversely [39]. This let us hypothesize that IGF-1 may stimulate endocytic recycling of HCN4. In line with this idea, the IGF-1 induced increase in HCN4 current was sensitive to dominant-negative Rab11 (Rab11 S25N). Also, dominant-negative dynamin (Dyn K44A), preventing canonical clathrin-dependent endocytosis, diminished the IGF-1 induced enhancement of HCN4 current. These observations were reproduced in the respective phospho-mimicking (SD) and phospho-ablative (SA) HCN4 mutants, strongly supporting the hypothesized signaling pathway. Whether and how N-terminal phosphorylation of HCN4 may improve its specific recruitment into Rab11-positive recycling endosomes, must remain elusive at this point. Somewhat surprising, however, neither wildtype HCN4 nor the phospho-ablative mutant currents were significantly affected by dominant-negative dynamin (Dyn K44A) under control conditions. According to the above mathematical model [39], a decline in the endocytic rate of HCN4 channels was expected to also enlarge their surface pool. We interpret this observation as a consequence of compensatory upregulation of dynamin-independent endocytotic trafficking, which might be associated with the caveolar localization of HCN channels [40,41]. Despite the two phospho-mutants largely anticipated the trafficking behavior of HCN4 channels in the presence or absence of IGF-1 signaling, respectively, still a residual response of increasing transmembrane current was observed upon IGF-1 application for both of them. This may indicate alternative IGF-1 signal transduction, *e.g. trans*-signaling *via* the RTK epidermal growth factor receptor (EGFR) eventually stimulating Rab11-dependent recycling without cargo specificity [42–44]. There may as well exist other IGF-1 dependent post-translational modifications of HCN4 besides phosphorylation of respective serine residues.

The here presented results extend the great complexity of PI3K signaling on I_f. It has previously been reported that pharmacological inhibition of PI3K may decrease I_f and slow spontaneous firing in rabbit SAN [45,46]. The authors hypothesized that downstream inhibition of AKT-dependent C-terminal phosphorylation of HCN2, shifting its voltage-dependent activation toward hyperpolarization, was one of the underlying molecular events. Surprisingly, AKT inhibition failed to mimick PI3K inhibition in rabbit SAN [46]. While caution must generally be exercised when translating conclusions from heterologous expression systems into native tissue, isoform- and hence species-specific differences should also be considered when interpreting data on native I_f. In good agreement with the here presented results, the serine/threonine phosphatase inhibitor calyculin A increased I_f conductance in native SAN cells without changing its voltage-dependent gating and on a similar time course as IGF-1 promoted cell surface expression of HCN4 [47].

Despite their predominant expression in cardiac pacemaker cells, HCN channels are also found in atrial and ventricular myocytes [22]. In a mouse model of cardiac hypertrophy, upregulation of ventricular I_f was linked to a diminished repolarization reserve and an increase in arrhythmogenic potential [48]. The authors showed a selective upregulation of HCN1, which by itself on a combined HCN2/4 knockout background failed to reproduce the phenotype of prolonged AP duration. It was therefore speculated that channel heteromerization may explain the observed increase in ventricular I_f. With IGF-1 as an important mediator of cardiac hypertrophy [49], the present study extends the view of heteromeric channel assembly, featuring a whole range of gating and trafficking characteristics, which are consecutively even subject to isoform-specific signal transduction, as a key mechanism for fine-tuning the properties of the cardiac pacemaker current in both physiology and pathophysiology.

CRediT authorship contribution statement

Nadine Erlenhardt: Writing – review & editing, Writing – original draft, Supervision, Formal analysis, Data curation, Conceptualization. **Franziska Wohlfarth:** Writing – review & editing, Investigation, Formal analysis. **S. Erfan Moussavi-Torshizi:** Writing – review & editing, Methodology, Investigation, Formal analysis, Data curation. **Angela Koch:** Writing – review & editing, Investigation, Formal analysis, Data curation. **Tobias Strasdeit:** Writing – review & editing, Investigation, Formal analysis, Data curation. **Katharina Scherschel:** Writing – review & editing, Conceptualization. **Ehsan Amin:** Writing – review & editing, Supervision, Methodology, Investigation. **Max Anstötz:** Writing – review & editing, Investigation. **Christian Meyer:** Writing – review & editing, Supervision, Methodology. **Nikolaj Klöcker:** Writing – review & editing, Writing – original draft, Project administration, Funding acquisition, Conceptualization.

Declaration of generative AI and AI-assisted technologies in the writing process

No AI-assisted technology was used in the preparation of this work.

Funding

The study was supported by the Deutsche Forschungsgemeinschaft (CRC1116, TPA01 to N.K.).

Declaration of competing interest

The authors declare no competing interests.

Acknowledgements

The authors thank O. Kletke and J. Gleich for methodological and technical support, respectively. The authors gratefully acknowledge the Center for Advanced Imaging (CAi) at Heinrich Heine University Düsseldorf for providing access to confocal microscopy.

Appendix A. Supplementary data

Supplementary data to this article can be found online at https://doi.org/10.1016/j.yjmcc.2025.10.015.

References

[1] P. De Meyts, J. Whittaker, Structural biology of insulin and IGF1 receptors: implications for drug design, Nat. Rev. Drug Discov. 1 (10) (2002) 769–783.
[2] R. Troncoso, C. Ibarra, J.M. Vicencio, E. Jaimovich, S. Lavandero, New insights into IGF-1 signaling in the heart, Trends Endocrinol. Metab. TEM 25 (3) (2014) 128–137.
[3] A. Clerk, P.H. Sugden, The insulin receptor family in the heart: new light on old insights, Biosci. Rep. 42 (7) (2022).
[4] O. Saetrum Opgaard, P.H. Wang, IGF-I is a matter of heart, Growth Hormone IGF Res. Off. J. Growth Hormone Res. Soc. Int. IGF Res. Soc. 15 (2) (2005) 89–94.
[5] Z. Ungvari, A. Csiszar, The emerging role of IGF-1 deficiency in cardiovascular aging: recent advances, J. Gerontol. Ser. A Biol. Sci. Med. Sci. 67 (6) (2012) 599–610.
[6] X. Lu, F. Kambe, X. Cao, M. Yamauchi, H. Seo, Insulin-like growth factor-I activation of Akt survival cascade in neuronal cells requires the presence of its cognate receptor in caveolae, Exp. Cell Res. 314 (2) (2008) 342–351.
[7] R. Troncoso, J.M. Vicencio, V. Parra, A. Nemchenko, Y. Kawashima, A. Del Campo, B. Toro, P.K. Battiprolu, P. Aranguiz, M. Chiong, S. Yakar, T.G. Gillette, J.A. Hill, E.

D. Abel, D. Leroith, S. Lavandero, Energy-preserving effects of IGF-1 antagonize starvation-induced cardiac autophagy, Cardiovasc. Res. 93 (2) (2012) 320–329.
[8] V. Eisner, A. Criollo, C. Quiroga, C. Olea-Azar, J.F. Santibañez, R. Troncoso, M. Chiong, G. Díaz-Araya, R. Foncea, S. Lavandero, Hyperosmotic stress-dependent NFkappaB activation is regulated by reactive oxygen species and IGF-1 in cultured cardiomyocytes, FEBS Lett. 580 (18) (2006) 4495–4500.
[9] D. Perkel, J. Naghi, M. Agarwal, R.P. Morrissey, A. Phan, R.D. Willix Jr., E. R. Schwarz, The potential effects of IGF-1 and GH on patients with chronic heart failure, J. Cardiovasc. Pharmacol. Ther. 17 (1) (2012) 72–78.
[10] S.F. Kemp, Insulin-like growth factor-I deficiency in children with growth hormone insensitivity: current and future treatment options, BioDrugs Clin. Immunotherap. Biopharm. Gene Ther. 23 (3) (2009) 155–163.
[11] D. Ley, B. Hallberg, I. Hansen-Pupp, C. Dani, L.A. Ramenghi, N. Marlow, K. Beardsall, F. Bhatti, D. Dunger, J.D. Higginson, A. Mahaveer, O.J. Mezu-Ndubuisi, P. Reynolds, C. Giannantonio, M. van Weissenbruch, N. Barton, A. Tocoian, M. Hamdani, E. Jochim, A. Mangili, J.K. Chung, M.A. Turner, L.E. H. Smith, A. Hellström, rhIGF-1/rhIGFBP-3 in preterm infants: a phase 2 randomized controlled trial, J. Pediatr. 206 (2019) 56–65.e8.
[12] M.M. Rutter, B.L. Wong, J.J. Collins, H. Sawnani, M.D. Taylor, P.S. Horn, P. F. Backeljauw, Recombinant human insulin-like growth factor-1 therapy for 6 months improves growth but not motor function in boys with Duchenne muscular dystrophy, Muscle Nerve 61 (5) (2020) 623–631.
[13] E.J. Gallagher, D. LeRoith, The proliferating role of insulin and insulin-like growth factors in cancer, Trends Endocrinol. Metab. 21 (10) (2010) 610–618.
[14] P.E. Vos, H.P. Koppeschaar, W.R. de Vries, J.H. Wokke, Insulin-like growth factor-I: clinical studies, Drugs Today (Barcelona, Spain 1998) 34 (1) (1998) 79–90.
[15] M.A. Hussain, O. Schmitz, A. Mengel, A. Keller, J.S. Christiansen, J. Zapf, E. R. Froesch, Insulin-like growth factor I stimulates lipid oxidation, reduces protein oxidation, and enhances insulin sensitivity in humans, J. Clin. Invest. 92 (5) (1993) 2249–2256.
[16] E. Vlachopapadopoulou, J.J. Zachwieja, J.M. Gertner, D. Manzione, D.M. Bier, D. E. Matthews, A.E. Slonim, Metabolic and clinical response to recombinant human insulin-like growth factor I in myotonic dystrophy–a clinical research center study, J. Clin. Endocrinol. Metab. 80 (12) (1995) 3715–3723.
[17] N. Cao, S. Lau, T.T. Nguyen, P.J. White, Characterization of the acute cardiovascular effects of intravenously administered insulin-like growth factor-I in conscious Sprague-Dawley rats, Clin. Exp. Pharmacol. Physiol. 33 (12) (2006) 1190–1195.
[18] M.F. Walsh, M. Barazi, G. Pete, R. Muniyappa, J.C. Dunbar, J.R. Sowers, Insulin-like growth factor I diminishes in vivo and in vitro vascular contractility: role of vascular nitric oxide, Endocrinology 137 (5) (1996) 1798–1803.
[19] G. Pete, Y. Hu, M. Walsh, J. Sowers, J.C. Dunbar, Insulin-like growth factor-I decreases mean blood pressure and selectively increases regional blood flow in normal rats, Proc. Soc. Exp. Biol. Med. Soc. Exp. Biol. Med. (New York, N.Y.) 213 (2) (1996) 187–192.
[20] M.E. Mangoni, J. Nargeot, Genesis and regulation of the heart automaticity, Physiol. Rev. 88 (3) (2008) 919–982.
[21] D. DiFrancesco, J.S. Borer, The funny current: cellular basis for the control of heart rate, Drugs 67 (Suppl. 2) (2007) 15–24.
[22] M. Baruscotti, A. Barbuti, A. Bucchi, The cardiac pacemaker current, J. Mol. Cell. Cardiol. 48 (1) (2010) 55–64.
[23] K. Hennis, C. Piantoni, M. Biel, S. Fenske, C. Wahl-Schott, Pacemaker channels and the chronotropic response in health and disease, Circ. Res. 134 (10) (2024) 1348–1378.
[24] S.E. Moussavi-Torshizi, E. Amin, N. Klöcker, Sex-specific repolarization heterogeneity in mouse left ventricle: optical mapping combined with mathematical modeling predict the contribution of specific ionic currents, Physiol. Rep. 11 (11) (2023) e15670.
[25] S. Fenske, R. Pröbstle, F. Auer, S. Hassan, V. Marks, D.H. Pauza, M. Biel, C. Wahl-Schott, Comprehensive multilevel in vivo and in vitro analysis of heart rate fluctuations in mice by ECG telemetry and electrophysiology, Nat. Protoc. 11 (1) (2016) 61–86.
[26] N. Hardel, N. Harmel, G. Zolles, B. Fakler, N. Klocker, Recycling endosomes supply cardiac pacemaker channels for regulated surface expression, Cardiovasc. Res. 79 (1) (2008) 52–60.
[27] K. Scherschel, H. Bräuninger, A. Mölders, N. Erlenhardt, E. Amin, C. Jungen, U. Pape, D. Lindner, D.M. Chetkovich, N. Klöcker, C. Meyer, Characterization of the HCN interaction partner TRIP8b/PEX5R in the intracardiac nervous system of TRIP8b-deficient and wild-type mice, Int. J. Mol. Sci. 22 (9) (2021).
[28] A. Girnita, L. Girnita, F. del Prete, A. Bartolazzi, O. Larsson, M. Axelson, Cyclolignans as inhibitors of the insulin-like growth factor-1 receptor and malignant cell growth, Cancer Res. 64 (1) (2004) 236–242.
[29] M. Reinartz, A. Raupach, W. Kaisers, A. Godecke, AKT1 and AKT2 induce distinct phosphorylation patterns in HL-1 cardiac myocytes, J. Proteome Res. 13 (10) (2014) 4232–4245.
[30] A.V. Glukhov, V.V. Fedorov, M.E. Anderson, P.J. Mohler, I.R. Efimov, Functional anatomy of the murine sinus node: high-resolution optical mapping of ankyrin-B heterozygous mice, Am. J. Physiol. Heart Circ. Physiol. 299 (2) (2010) H482–H491.
[31] R. Seifert, A. Scholten, R. Gauss, A. Mincheva, P. Lichter, U.B. Kaupp, Molecular characterization of a slowly gating human hyperpolarization-activated channel predominantly expressed in thalamus, heart, and testis, Proc. Natl. Acad. Sci. U. S. A. 96 (16) (1999) 9391–9396.
[32] P. Pian, A. Bucchi, R.B. Robinson, S.A. Siegelbaum, Regulation of gating and rundown of HCN hyperpolarization-activated channels by exogenous and endogenous PIP2, J. Gen. Physiol. 128 (5) (2006) 593–604.
[33] G. Zolles, N. Klöcker, D. Wenzel, J. Weisser-Thomas, B.K. Fleischmann, J. Roeper, B. Fakler, Pacemaking by HCN channels requires interaction with phosphoinositides, Neuron 52 (6) (2006) 1027–1036.
[34] H. Jo, S. Mondal, D. Tan, E. Nagata, S. Takizawa, A.K. Sharma, Q. Hou, K. Shanmugasundaram, A. Prasad, J.K. Tung, A.O. Tejeda, H. Man, A.C. Rigby, H. R. Luo, Small molecule-induced cytosolic activation of protein kinase Akt rescues ischemia-elicited neuronal death, Proc. Natl. Acad. Sci. U. S. A. 109 (26) (2012) 10581–10586.
[35] B.D. Manning, A. Toker, AKT/PKB signaling: navigating the network, Cell 169 (3) (2017) 381–405.
[36] N. Balasuriya, N.E. Davey, J.L. Johnson, H. Liu, K.K. Biggar, L.C. Cantley, S.S. Li, P. O'Donoghue, Phosphorylation-dependent substrate selectivity of protein kinase B (AKT1), J. Biol. Chem. 295 (24) (2020) 8120–8134.
[37] Z. Liao, D. Lockhead, E.D. Larson, C. Proenza, Phosphorylation and modulation of hyperpolarization-activated HCN4 channels by protein kinase A in the mouse sinoatrial node, J. Gen. Physiol. 136 (3) (2010) 247–258.
[38] T. Welz, J. Wellbourne-Wood, E. Kerkhoff, Orchestration of cell surface proteins by Rab11, Trends Cell Biol. 24 (7) (2014) 407–415.
[39] K.E. Shipman, K.R. Long, I.A. Cowan, Y. Rbaibi, C.J. Baty, O.A. Weisz, An adaptable physiological model of endocytic megalin trafficking in opossum kidney cells and mouse kidney proximal tubule, Function (Oxford, England) 3 (6) (2022) zqac046.
[40] R.G. Parton, J.W. Taraska, R. Lundmark, Is endocytosis by caveolae dependent on dynamin? Nat. Rev. Mol. Cell Biol. 25 (7) (2024) 511–512.
[41] A. Barbuti, B. Gravante, M. Riolfo, R. Milanesi, B. Terragni, D. DiFrancesco, Localization of pacemaker channels in lipid rafts regulates channel kinetics, Circ. Res. 94 (10) (2004) 1325–1331.
[42] F.L. Roudabush, K.L. Pierce, S. Maudsley, K.D. Khan, L.M. Luttrell, Transactivation of the EGF receptor mediates IGF-1-stimulated shc phosphorylation and ERK1/2 activation in COS-7 cells, J. Biol. Chem. 275 (29) (2000) 22583–22589.
[43] A. Wallroth, V. Haucke, Phosphoinositide conversion in endocytosis and the endolysosomal system, J. Biol. Chem. 293 (5) (2018) 1526–1535.
[44] C.C. Campa, J.P. Margaria, A. Derle, M. Del Giudice, M.C. De Santis, L. Gozzelino, F. Copperi, C. Bosia, E. Hirsch, Rab11 activity and PtdIns(3)P turnover removes recycling cargo from endosomes, Nat. Chem. Biol. 14 (8) (2018) 801–810.
[45] R.Z. Lin, Z. Lu, E.P. Anyukhovsky, Y.P. Jiang, H.Z. Wang, J. Gao, M.R. Rosen, L. M. Ballou, I.S. Cohen, Regulation of heart rate and the pacemaker current by phosphoinositide 3-kinase signaling, J. Gen. Physiol. 151 (8) (2019) 1051–1058.
[46] Z. Lu, H.Z. Wang, C.R. Gordon, L.M. Ballou, R.Z. Lin, I.S. Cohen, Regulation of HCN2 current by PI3K/Akt signaling, Front. Physiol. 11 (1443) (2020).
[47] E.A. Accili, G. Redaelli, D. DiFrancesco, Differential control of the hyperpolarization-activated current (i(f)) by cAMP gating and phosphatase inhibition in rabbit sino-atrial node myocytes, J. Physiol. 500 (Pt 3) (1997) 643–651.
[48] F. Hofmann, L. Fabritz, J. Stieber, J. Schmitt, P. Kirchhof, A. Ludwig, S. Herrmann, Ventricular HCN channels decrease the repolarization reserve in the hypertrophic heart, Cardiovasc. Res. 95 (3) (2012) 317–326.
[49] W.S. Lee, E.D. Abel, J. Kim, New insights into IGF-1 signaling in the heart, Physiology (Bethesda) 39 (5) (2024).